Low velocity perforation of an aluminum alloy: experiments and simulations

Léonard Antoinat[1,*], Régis Kubler[1], Guillaume Achard[1], Jean-Luc Barou[2], Philippe Viot[2], Laurent Barrallier[1]

[1] MSMP, Arts et Métiers ParisTech, 13617 Aix en Provence, France
[2] Arts et Métiers ParisTech, I2M, UMR 5295, 33405 Talence, France
* Corresponding author: leonard.antoinat@ensam.eu

Abstract Low velocity perforation of an aeronautical aluminum alloy sheet 2024 T3 subjected to impact is studied in this paper. The main objective is to compare experimental results and simulations by analysis of the failure. The perforation test is made with an instrumented 3 meter drop test. The striker has a large diameter (45 mm) and a conical shape. Sheets' thickness is 2 mm. The influence of the impact velocity is analyzed. A phenomenological behavior law of the sheet's material is implemented in the finite element code Abaqus/Explicit. Thus, 3D simulations of perforation are performed using a damage evolution law and a ductile failure criterion. To understand the phenomenon, the perforation force and the sticker velocity will be analyzed. Simulations are validated by experimental tests and compared with an analytical model.
Keywords Dynamic perforation, Aluminum, Experiments, FE Simulations, Analytical perforation model

1. Introduction

An increased attention in impact issues is paid by authors working on various engineering fields like aeronautic [1], naval [2], and automotive [3]. Impact on ductile material involves high strain rates effects [4] and temperature effects [5]. Thus, the knowledge of material dynamic behavior is necessary. Particular constitutive laws are known to be adapted for this type of issue [6]. The ductile target perforation is a specific case of impact studies. Perforation tests can be classified in categories according to the test velocity is high [7] or low [8], or according to the different striker's geometries (diameter, nose shape,…). An energetic approach is recommended to understand perforation issue. The energy absorbed by the target during impact E_a can be calculated using the difference between the initial kinetic energy and the final kinetic energy [8]. The ballistic limit V_{bl} is known to be the minimal initial velocity involving perforation. In order to have a better understanding of the rupture phenomenon and in order to compare with simulation results, it is necessary to know the force applied to the target and/or the striker displacement, during impact. This is the reason why some authors use the Hopkinson bar theory [9] [10] or an instrumented pneumatic accelerator or drop test [9] to be able to plot the curve of the force versus the time and/or the displacement. Low velocity perforation of an aeronautical aluminum alloy sheet 2024 T3 subjected to impact is studied in this paper. Unlike Rodriguez-Martinez [8] who studied the perforation of thin target (1 mm), the idea is here to work with thicker plates (2 mm) and with a larger striker (45 mm).

A two-pronged approach for perforation is proposed here: an experimental approach with the use of a drop test and a modeling approach including a finite element (FE) approach and an analytical approach. Results are compared and discussed.

2. Drop test: Perforation of 2024 T3 aluminum alloy sheets

2.1. Material

Aluminum alloys are known for their high mechanical characteristics against their density. The 2024 T3 aluminum alloy (2024 AA) is used in aeronautical structural parts as planes' fuselage or wings. The process route of this precipitation hardening material, alloyed with copper, is well known: a casting, a homogenizing, a hot rolling, a solute heat treatment at 495°C, a water quench, a cold work to obtain higher strain, and to finish a natural aging. This is the T3 heat treatment [11]. The chemical composition of the 2024 aluminum alloy is presented in Table 1.

Table 1. Chemical composition in %wt of the 2024 AA [12].

Al	Cu	Mg	Mn	Fe	Si	Zn	Ti	Cr
Bal.	4.76	1.38	0.65	0.22	0.08	0.07	0.03	0.01

2.2. Experimental setup

An instrumented drop test is used to perforate 2024 AA sheets (Fig. 1). A 5 kg test trolley slides on two bars from various height positions. Weights can be added to this trolley. Under the trolley a piezoelectric force sensor and a conical striker are fixed. This dynamic force sensor is calibrated for a range of validity from 0 to 100 kN and is used to measure the perforation force during impact with a relative error less than 5%. The striker is composed of a 60° conical nose and a 45 mm diameter cylindrical part. This cylindrical part is 10 mm long. A laser sensor (error of 0.5%) is used to measure the trolley's displacement. Two high speed cameras are used to measure the striker displacement and to take picture of the sheet's perforation. A mirror enables the observation beneath the sheet.

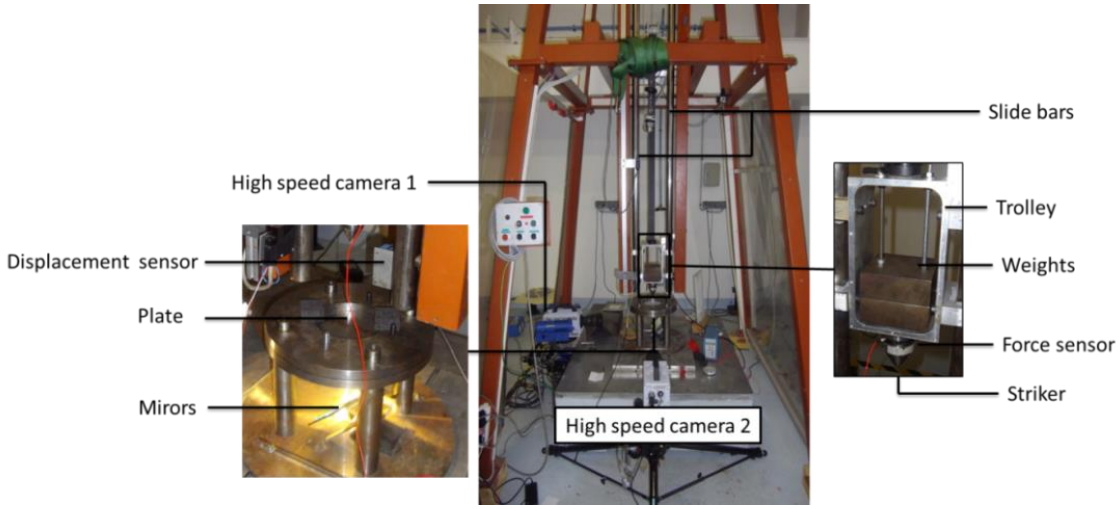

Figure 1. Instrumented drop test.

Twelve drop tests are performed to perforate a 2 mm 2024 AA sheet. The initial impact velocity and the striker total mass of each test are given in Table 2. If the striker perforates the sheet, values are in bolt font. The impact velocity evolves from 2.7 m/s to 6.9 m/s. The striker total mass is taken equal to 13 kg. The main objective is to find the ballistic limit velocity, to study the residual velocity and to analyze fracture and the force during impact.

2.3. Experimental results

2.3.1. Description of the perforation test

A 2 mm 2024 AA sheet is impacted by the striker. Thus, the striker nose induces plastic strain in the center of the sheet. More than four cracks appear, two in the laminated direction, two in the transversal direction, and sometimes in the 45° direction (Table 2). If the conical nose does not go through the plate, the striker bounces. If the conical nose goes through the sheet, the force sensor hits the sheet involving a bounce. All are analyzed before this bounce.

Table 2. Testing plan and main results.

Test number	1	2	3	4	5	6	**7**	**8**	**9**	**10**	**11**	**12**
Total mass (kg)	13	13	13	13	13	13	**13**	**13**	**13**	**13**	**13**	**13**
Drop test height (m)	0.4	0.4	1	1	1.5	1.5	**1.8**	**1.8**	**2**	**2**	**2.2**	**2.5**
Impact velocity (m/s)	2.79	2.71	4.24	4.20	5.00	4.81	**5.52**	**5.58**	**5.72**	**5.82**	**6.30**	**6.90**
Petals number	4	4	5	5	6	4	**6**	**5**	**4**	**4**	**6**	**5**
Residual velocity (m/s)	-1.4	-1.3	-1.3	-1.5	-1.3	-1.1	**2.6**	**3.2**	**2.6**	**2.6**	**4.0**	**4.6**
Absorbed Energy (J)	51	48	117	115	163	150	**155**	**160**	**168**	**152**	**157**	**170**
Peak Force (kN)	8.7	8.4	9.1	8.8	10.0	9.2	**9.3**	**9.5**	**9.5**	**9.2**	**9.2**	**Unknown**
Maximal Force (kN)	6.6	7.1	8.2	8.6	9.4	9.4	**9.6**	**9.4**	**9.9**	**9.6**	**9.6**	**Unknown**

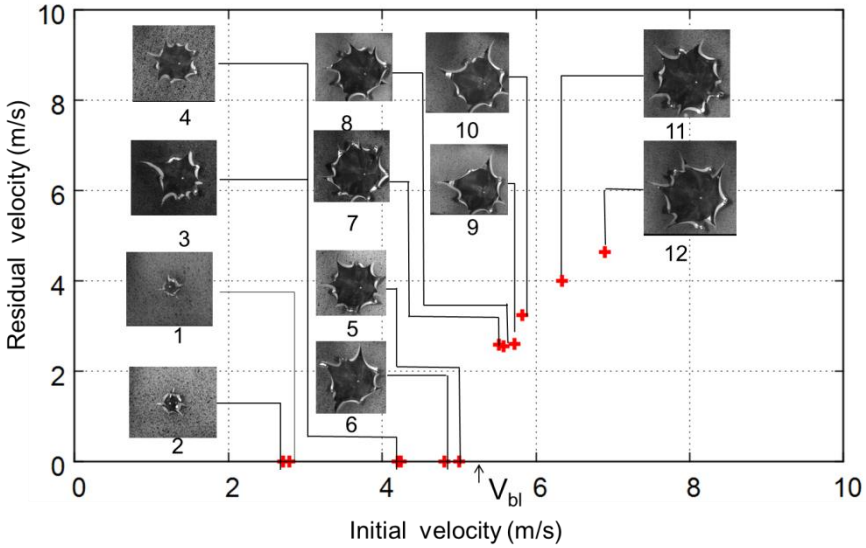

Figure 2. Residual velocity versus initial velocity.

2.3.2. Velocity results

It is usual to plot the residual velocity of the striker as a function of the initial velocity. In Fig. 2, if the striker does not perforate the sheet completely, the residual velocity is taken equal to 0. Classical results show that starting from the ballistic limit the velocity V_{bl} is a continuous growing curve [8]. Here this hypothesis is confirmed. In Fig. 2, pictures are taken at the end of the perforation (before the bounce). Thus it can be concluded, that using a 13 kg conical striker, the ballistic limit velocity to perforate a 2 mm sheet of 2024 AA is between 5 and 5.52 m/s. To obtain a better approximation of the ballistic limit velocity, the definition of the absorbed energy during perforation is used. This

energy is calculated as the difference between the initial kinetic energy and the final one and given in Table 2 for each test. The ballistic limit velocity V_{bl} can be estimated using the average absorbed energy E_a = 161 J as:

$$V_{bl} = \sqrt{\frac{2E_a}{m_{striker}}} \quad , m_{striker} = 13kg \tag{1}$$

It can be concluded that the ballistic limit velocity is equal to 5.0 m/s with an error of +/- 3%.

2.3.3. Force during impact

The force induced by the sheet on the striker can be plot during impact with the help of the force sensor (Fig. 6). Firstly, when the striker is reaching the sheet, a force peak can be observed. Secondly, cracks appear and so the force is continuously growing to be maximal when the striker cylindrical part is reached (test 7 to 12) or when the striker start to bounce back (test 1 to 6). After, the force is decreasing. If the conical nose goes through the sheet, the force sensor will hit the sheet involving a new increase of force.

2.4. Conclusion on experimental results

It can be concluded that the ballistic limit velocity is about 5 m/s +/- 3% using a 13 kg striker. Four or more than four petals always appear in the sheet during perforation. The perforation absorbed energy tends to be constant and equal to 161 J for impact velocity between 5 m/s and 7 m/s.

3. Modeling of perforation

Experimental tests are compared with two models: an analytical model based on energetic consideration and a shell finite elements model.

3.1 Perforation analytical model

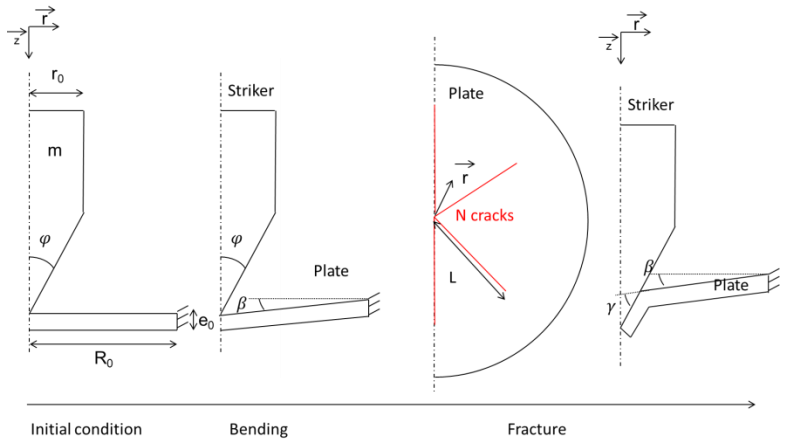

Figure 3. Analytical model.

An energetic approach for perforation is proposed by Nazeer [13]. A conical nose striker impacting thin plates involves bending deformation, stretching deformation and N cracks' propagation (fig 3).

The idea is to adapt this model in order to study the ballistic limit velocity and the residual velocity of the striker and with the hypothesis that the radius of the dimple is equal to the sheet radius. The elastic bending work is neglected. Thus, the total perforation work W is the sum of the bending plastic work W_b the stretching plastic work W_s, the petals' bending work W_{bf} and the fracture work W_f ($W = W_b + W_s + W_{bf} + W_f$). The perforation work is the absorbed energy and so with the definition of the absorbed energy, the residual velocity V_r is given as a function of the initial velocity V_0:

$$W = \frac{1}{2} m_{striker}(V_0^2 - V_r^2) \quad \rightarrow \quad V_r = \sqrt{V_0^2 - \frac{2W}{m_{striker}}} = \sqrt{V_0^2 - \frac{2(W_b+W_s+W_{bf}+W_f)}{m_{striker}}} \tag{2}$$

To obtain the ballistic limit velocity, the initial velocity is taken equal to V_{bl} and the residual velocity V_r equal to 0 m/s. Thus, we obtain:

$$V_{bl} = \sqrt{\frac{2W}{m_{striker}}} = \sqrt{\frac{2(W_b+W_s+W_{bf}+W_f)}{m_{striker}}} \tag{3}$$

where

- the bending work W_b is given as a function of the yield stress σ_y, the initial thickness e_0 the sheet's radius R_0 and the bending angle β (calculated as a function R_0 and the striker displacement z as $\tan(\beta) = \frac{z}{R0}$). by:
$$W_b = \pi \sigma_y e_0^2 R_0 \beta \tag{4}$$
- the stretching work W_s of the sheet is given as a function of the yield stress σ_y, e_0, R_0, and the stretching strain ε_s by $W_s = (\pi R_0)^2 \sigma_y e_0 \ \varepsilon_s$. The stretching strain can be defined thanks to the evolving surface area of the sheet and its original area $\left(\varepsilon_s = \ln\left(\sqrt{R_0^2 - z^2}/R_0\right)\right)$:
$$W_s = (\pi R_0)^2 \sigma_y e_0 \ \ln\left(\sqrt{\frac{R_0^2 - z^2}{R_0^2}}\right) \tag{5}$$
- the bending work W_{bf} involved by each petals can be written as a function of the number of petals N, the striker radius r_0, the thickness e, and γ the petals bending angle ($\gamma = \frac{\pi}{2} - \varphi - \beta$) as (see Fig. 3):
$$W_{bf} = \frac{\pi \sigma_y r_0 e^2 \gamma}{2} \frac{2+N}{1+N} \tag{6}$$
- the Fracture work W_f is due to crack propagation. It can be given as a function of the fracture toughness G, the thickness e and the length of fracture L by $W_f = NGeL$.The thickness e can be express with the stretching strain as $e = e_0/\sqrt{1 + z_b/R_0^2}$. L is taken equal to the projection of the striker on the bending sheet ($L = \sqrt{r_0^2 + z_b^2}$). The parameter z_b, is the ultimate bending striker displacement the parameter. Thus the fracture work is given by :
$$W_f = NGe_0 \ln\left(\sqrt{\frac{R_0^2 - z_b^2}{R_0^2}}\right)\sqrt{r_0^2 + z_b^2} \tag{7}$$

Here the angle of the conical striker is 60°, its mass is equal to 13 kg, and its diameter is 45 mm. The sheet thickness is 2 mm and its diameter is 148 mm. The static yield stress is $\sigma_y = 340\ MPa$, the number of petals is taken equal to 4 and the ultimate bending striker displacement z_b is 3 mm.

3.2 Finite element model for perforation

3.2.1 Material behavior law of 2024 T3 AA

A classical Johnson Cook behavior law [6] is used in the finite element code Abaqus [14] to model the viscoplastic behavior where A, B, n, m, C and $\dot{\varepsilon}_0$ are material parameters, Tmelt is the melt temperature and Troom is the room temperature. The stress σ can also be written as a function of the plastic strain ε^p , the plastic strain rate $\dot{\varepsilon}^p$, and the temperature T :

$$\sigma = \left(A + B\varepsilon^{p\,n}\right)\left(1 + Cln\left(\frac{\dot{\varepsilon^p}}{\dot{\varepsilon_0}}\right)\right)\left(1 - \left(\frac{T-T_{room}}{T_{melt}-T_{room}}\right)^m\right) \tag{8}$$

The elastic behavior is isotropic (E=74 GPa, ν=0.3). Above a plastic strain threshold, voids appear, grow and coalesce in the material, to produce the rupture [15]. To define this damage, a damage variable D is used in the model. The evolution of D can be written using the Johnson Cook dynamic damage model [16]. The damage D is dependent on the plastic strain rate, materials parameters m, D1, D2, D3¸D4 and D5, the hydrostatic pressure p, the equivalent stress σ_{eq}, the melt temperature Tmelt and the room temperature Troom :

$$\dot{D} = \frac{\dot{\varepsilon^p}}{\varepsilon_R} = \frac{\dot{\varepsilon^p}}{\left(D_1 + D_2\, e^{\frac{D_3 p}{\sigma eq}}\right)\left(1 + D_4 ln\left(\frac{\dot{\varepsilon^p}}{\dot{\varepsilon_0}}\right)\right)\left(1 - D_5\left(\frac{T-T_{room}}{T_{melt}-T_{room}}\right)^m\right)} \tag{9}$$

Lesuer [12] used an isotropic Johnson Cook hardening and a Johnson Cook rupture model for a 2024 AA with the parameters presented in Table 3. The strain rate parameter $\dot{\varepsilon}_0$ is taken equal to $1s^{-1}$, T_{room} equals 298 K and T_{melt} equals 775 K. Parameters D_1 and D_2 are determined to predict the residual velocity after impact, according to the presented experiment. Because of the temperature dependence, the specific heat cp is taken equal to 897 J/kg/K, the inelastic heat fraction equal β to 0.9 and the conductivity equal to 237 W/m/K.

Table 3. Johnson Cook hardening and fracture law parameters [12] (**modified in bolt fonts**)

A (MPa)	B (MPa)	n	C	m	D_1	D_2	D_3	D_4	D_5
369	684	0.73	0.0083	1.7	**0.035**	**0.035**	-1.5	0.011	0.0

3.2.2 3D finite element model.

A 3D finite element simulation is carried out using ABAQUS/Explicit. Shell elements are known to be well adapted for solving thin sheets' perforation issues [17]. Thus the 2024 AA sheet is modeled with 3200 S4RT elements and 1869 S3RT elements with the JC law presented above (Table 3.) For stability reason, five integration points are taken in the sheet's thickness. An analytical rigid surface is used to model the conical striker. The trolley mass is applied on the striker reference point. Interaction between the striker and the sheet is modeled by a perfect contact (hard contact and frictionless). Elements are deleted when the damage D is equal to 1. The sheet is clamped at the edges. The initial velocity is applied on the striker reference point. The striker moves only along the vertical direction. Temperature effects are taken into account but will not be discussed here. Initial

velocities of simulations are taken similar to experimental drop tests (2.7 m/s, 4.2 m/s, 5 m/s, 5.5 m/s, 5.8 m/s, 6.3 m/s and 6.9 m/s) and another one equal to 8 m/s.

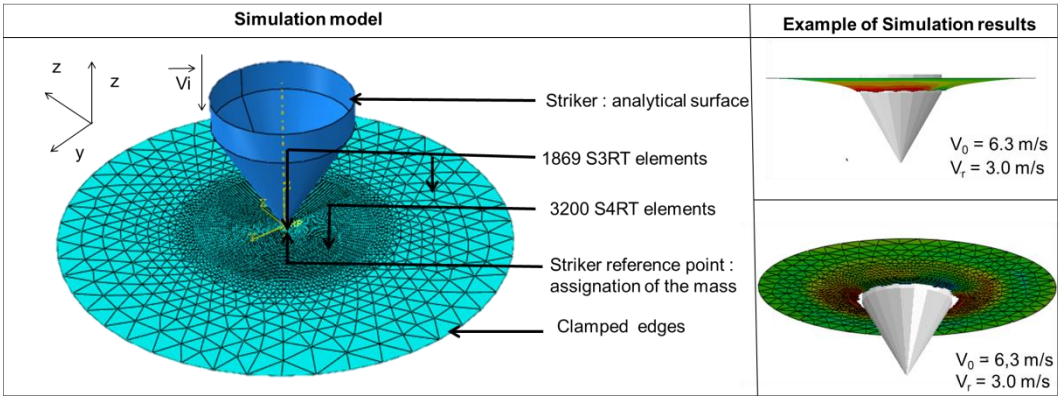

Figure 5. Shell finite elements model and simulation results.

4. Results and discussions

4.1. Perforation force

Drop tests force during impact is compared to numerical results. In Fig. 6, forces are plotted for an initial velocity of 5.8 m/s. Simulation's force is noised because of numerical instabilities. That's the reason why a centered average numerical force is plotted. It can be noticed that the first force peak is not simulated. The numerical model does not take in consideration friction effects and failure propagation and thus the numerical force underestimates the measured force. As the measured force, the numerical force rises during the perforation until a maximal force, equal to 8.8 kN, versus 9.6 kN for the measured force.

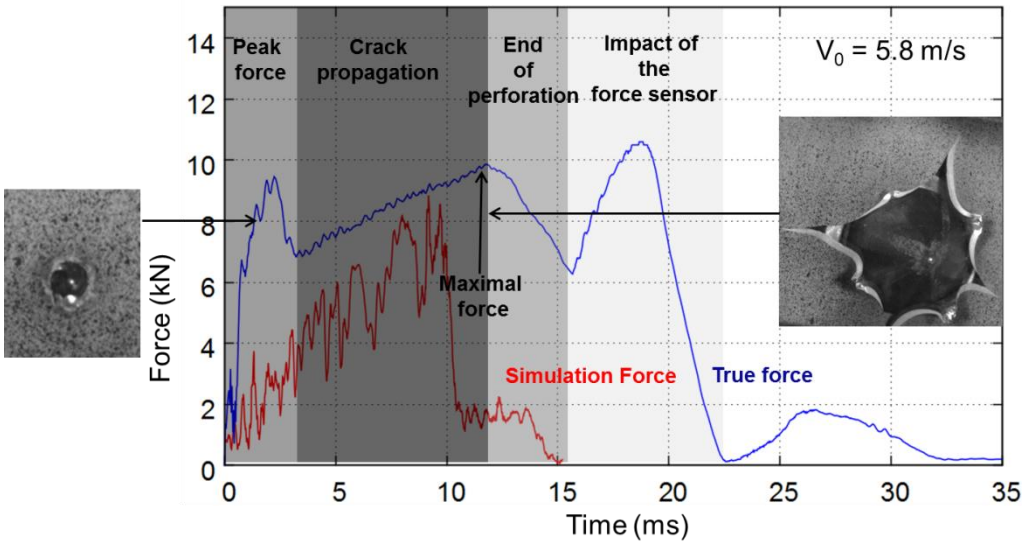

Figure 6. Force during impact versus time for an initial velocity of 5.8 m/s (test 9).

4.2. Discussion on the ultimate bending striker displacement before perforation

The ultimate bending striker displacement before perforation z_b, is used to calculate the residual velocity for the analytical model. It can be determined by drop tests' results and finite elements' results, and is equal to the displacement of the striker before rupture. For an initial velocity of 5.8 m/s, z_b is equal to 2.9 mm and 3.5 mm respectively for simulation and experiment. The hypothesis to take z_b equal to 3 mm for the analytical model is in good agreement.

4.3. Velocity discussions

Velocity's results are discussed by plotting the residual velocity as a function of the initial velocity (Fig. 7). Analytical model's results (N=4, z_b=3mm) are in good agreement with drop tests' results. Simulations tend to underestimate residual velocities, but results are close to experimental ones.

A good ballistic limit velocity correlation is found. With the analytical model, it is equal to 5.0 m/s. With the finite elements model, it is between 5 and 5.5 m/s. The experimental ballistic limit velocity is about 5.0 m/s.

Experimentally, the absorbed energy by the sheet during impact rises with the initial velocity until a maximal energy (about 161 J), reached for the ballistic limit velocity (Fig. 7). Drop tests' results give an average maximal absorbed energy for perforation of 161 J. In the analytical model, this maximal absorbed energy for perforation is the addition of plastic work and fracture work and is equal to 168 J. Because of the use of a rate dependent model, simulations show that the absorbed energy continues to rise beyond the ballistic limit velocity and exceeds 180 J.

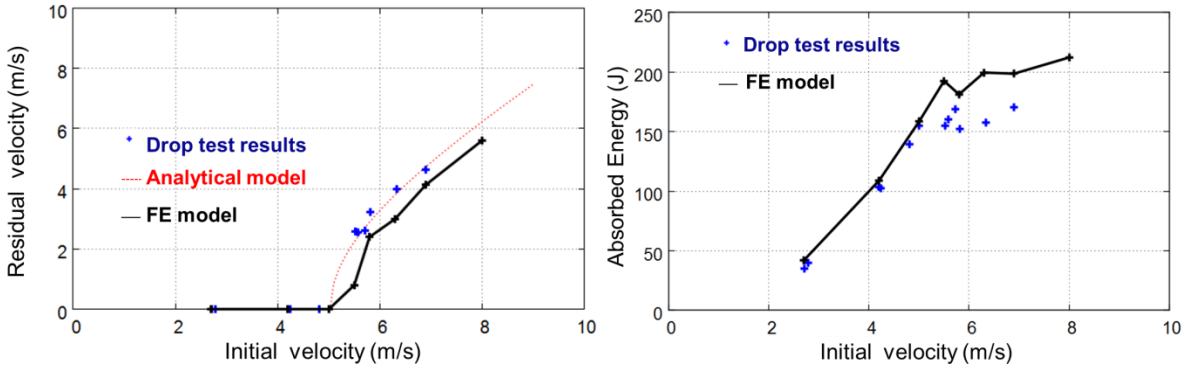

Figure 7. Residual velocity versus initial velocity and absorbed energy versus initial velocity.

4.4. Discussion on the number of petals.

More than four petals appear during perforation tests (Table 2). Because of the use of the "kill element" process, no petal is observed in FE simulations. It was already explained that results from the analytical model are number of cracks dependent. In this model, an evolution of the number of petals leads to an augmentation of the absorbed energy during impact and thus a decrease of the residual velocity. For example, for an initial velocity equal to 6.9 m/s the residual velocity is 4.7 m/s,

4.6 m/s and 4.5 m/s for respectively 4, 5 and 6 petals. This tendency is not confirmed by drop tests' results (Table. 2).

5. Conclusion and remarks

Thin sheets of 2024 AA were perforated, on a drop test, by a 60° and 45 mm diameter conical striker for a range of velocity from 2.7 m/s to 6.9 m/s. The energy needed to perforate is about 160 J. Four or more than four petals always appear in the sheet during perforation. A numerical model and an analytical model were proposed. Shell element model coupled with Johnson Cook viscoplastic and damage laws is adapted to simulate the perforation of thin sheet of aluminum alloy. The ballistic limit velocity, the residual velocity as well as the impact are in good agreement with experimental data. It can be shown that simulated force during impact is below the experimental force. The analytical model also predicts the residual velocity.

Simulations using an anisotropic material model for rolled sheets are underway and predict petals' formation during perforation (Fig. 8). Future analysis of pictures taken by high speed camera, beneath the sheet, will permit to perform image correlation for strain measurements in order to correlate the simulated strain field and the experimental strain field and therefore to better analyze the crack propagation (fracture criterion).

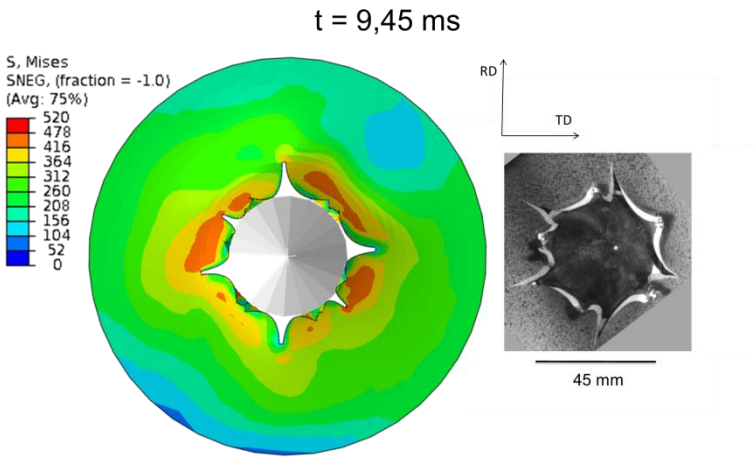

Figure 8. Simulation versus experiment for an initial velocity of 6.9 m/s using an anisotropic material model.

Acknowledgements

The financial support of this work from OSEO, a **s**tructure for the benefit of SMEs and innovation, is gratefully acknowledged.

References

[1] K. E. Jackson, R. L. Boitnott, E. L. Fasanella, L. E. Jones and K. H. Lyle, A History of Full-Scale Aircraft and Rotorcraft Crash Testing and Simulation at NASA Langley Research Center, 4th Triennial International Aircraft and Cabin Safety Research Conference, 2004.

[2] A. Tassin, Modélisation tridimensionnelle d'impacts hydrodynamiques pour l´étude du tossage des bulbes d´étrave., 2010.

[3] S. Hou, Q. Li, S. Long, X. Yang and W. Li, Multiobjective optimization of multi-cell sections for the crashworthiness design, International Journal of Impact Engineering, vol. 35, no. 11, pp. 1355-1367, 2008.

[4] G. Taylor, The Use of Flat-Ended Projectiles for Determining Dynamic Yield Stress. I. Theoretical Considerations, Proceedings of the Royal Society of London. Series A. Mathematical and Physical Sciences, vol. 194, no. 1038, pp. 289-299, 1948.

[5] R. J. Clifton, Response of materials under dynamic loading, International Journal of Solids and Structures, vol. 37, no. 1-2, pp. 105-113, 2000.

[6] G. R. Johnson and W. H. Cook, A constitutive model and data for metals subjected to large strains, high strain rates and high temperatures, Proceedings of the 7th International Symposium on Ballistics, vol. 547, no. 11, pp. 541-547, 1983.

[7] T. Borvik, A. H. Clausen, O. S. Hopperstad and M. Langseth, Perforation of AA5083-H116 aluminium plates with conical-nose steel projectiles : experimental study, International Journal of Impact Engineering, vol. 30, no. 4, pp. 367-384, 2004.

[8] J. Rodriguez-Martinez, A. Rusinek and A. Arias, Thermo-viscoplastic behaviour of 2024-T3 aluminium sheets subjected to low velocity perforation at different temperatures, Thin-Walled Structures, vol. 49, no. 7, pp. 819-832, 2011.

[9] F. Grytten, T. Borvik, O. Hopperstad and M. Langseth, Low velocity perforation of AA5083-H116 aluminium plates, International Journal of Impact Engineering, vol. 36, no. 4, pp. 597-610, 2009.

[10] M. Ramezani and Z. M. Ripin, Combined experimental and numerical analysis of bulge test at high strain rates using split Hopkinson pressure bar apparatus, Journal of Materials Processing Technology, vol. 210, no. 8, pp. 1061-1069, 2010.

[11] M. Stucky, Traitements thermiques des alliages d'aluminium, Les Techniques de l'Ingénieurs, vol. M 1 290v2, pp. 1-25, 1986.

[12] D. R. Lesuer, Experimentel Investigations of Material Models for Ti-6Al-4V Titanium and 2024-T3 Aluminum, Office of Aviation Research Washington, pp. 1-41, 2000.

[13] M. M. Nazeer, M. Khan, A. Naeem and A. u. Haq, Analysis of conical tool perforation of ductile metal sheets, International Journal of Mechanical Sciences, vol. 42, no. 7, pp. 1391-1403, 2000.

[14] Abaqus, Abaqus Analysis User's Manual, 2010.

[15] J. Lemaître and J. Chaboche, Mécanique des matériaux solides, Dunod, 1988.

[16] G. R. Johnson and W. H. Cook, Fracture characteristics of three metals subjected to various strains, strain rates, temperatures and pressures, Engineering Fracture Mechanics, vol. 21, no. 1, pp. 31-48, 1985.

[17] J. Dean, A. S-Fallah, P. Brown, L. Louca and T. Clyne, Energy absorption during projectile perforation of lightweight sandwich panels with metallic fibre cores, Composite Structures, vol. 93, no. 3, pp. 1089-1095, 2011.